THE ASTROPHYSICAL JOURNAL, 443:L57–L60, 1995 April 20

DEGREE-SCALE ANISOTROPY IN THE COSMIC MICROWAVE BACKGROUND: SP94 RESULTS

J. O. GUNDERSEN,[1,2] M. LIM,[1,2] J. STAREN,[1,2] C. A. WUENSCHE,[3] N. FIGUEIREDO,[1,3,4] T. C. GAIER,[1,2] T. KOCH,[5] P. R. MEINHOLD,[1,2] M. D. SEIFFERT,[1,2] G. COOK,[1] A. SEGALE,[1] AND P. M. LUBIN[1,2]

Received 1994 December 1; accepted 1995 February 8

ABSTRACT

We present results from two observations of the cosmic microwave background (CMB) performed from the South Pole during the 1993–1994 austral summer. Each observation employed a 3° peak-to-peak sinusoidal, single-difference chop and consisted of a 20° × 1° strip on the sky. The first observation used a receiver which operates in three channels between 38 and 45 GHz (Q-band) with a FWHM beam which varies from 1° to 1°.15. The second observation overlapped the first observation and used a receiver which operates in four channels between 26 and 36 GHz (Ka-band) with a FWHM beam which varies from 1°.5 to 1°.7. Significant correlated structure is observed in all channels for each observation. The spectrum of the structure is consistent with a CMB spectrum and is formally inconsistent with diffuse synchrotron and free-free emission at the 5 σ level. The amplitude of the structure is inconsistent with 20 K interstellar dust; however, the data do not discriminate against flat or inverted spectrum point sources. The root mean square amplitude ($\pm 1\ \sigma$) of the combined (Ka + Q) data is $\Delta T_{\rm rms} = 41.2^{+15.5}_{-6.7}\ \mu$K for an average window function which has a peak value of 0.97 at $\ell = 68$ and drops to $e^{-0.5}$ of the peak value at $\ell = 36$ and $\ell = 106$. A band power estimate of the CMB power spectrum, C_ℓ, gives $\langle C_\ell \ell(\ell + 1)/(2\pi)\rangle_B = 1.77^{+1.58}_{-0.54} \times 10^{-10}$.

Subject headings: cosmic microwave background — cosmology: observations

1. INTRODUCTION

Anisotropy measurements of the cosmic microwave background (CMB) are a very effective tool for testing and constraining models of cosmic structure formation. With the discovery of large angular anisotropy by *COBE* (Smoot et al. 1992), there has been an increased interest in characterizing anisotropy on degree angular scales. Although all CMB measurements have to overcome a long list of systematic effects and foreground contaminants (Wilkinson 1994), they have the potential to constrain many of the global parameters of the universe and thus discriminate among the plethora of cosmic structure formation models. Over the past 6 years, we have traveled to the South Pole 3 times to perform these degree-scale anisotropy measurements. The results from our 1988–1989 measurements are detailed in Meinhold & Lubin (1991) (SP89a) and Meinhold et al. (1993) (SP89b), while the results from the 1990–1991 measurements are detailed in Gaier et al. (1992) (SP91a) and Schuster et al. (1993) (SP91b). The results from these measurements and the five balloon-borne Millimeter-wave Anisotropy Experiment (MAX) are summarized in Lubin (1994). In order to obtain additional sky coverage and frequency coverage, we returned to the Amundsen-Scott South Pole Station during the austral summer 1993–1994 (SP94).

[1] Department of Physics, University of California, Santa Barbara, CA 93106.
[2] NSF Center for Particle Astrophysics, University of California, Berkeley, CA 94720.
[3] Instituto Nacional de Pesquisas Espaciais-INPE/MCT, Divisao de Astrofisica, Sao Jose dos Campos, SP, Brazil 12227-010.
[4] Escola Federal de Engenharia de Itajuba, Departamento de Fisica e Quimica, Itajuba, MG, Brazil 37500-000.
[5] Jet Propulsion Laboratory, California Institute of Technology, 4800 Oak Grove Drive, Pasadena, CA 91109.

2. INSTRUMENTATION

The SP94 observations used the Advanced Cosmic Microwave Explorer (ACME), as have all our previous degree-scale anisotropy measurements. ACME is a 1 m off-axis Gregorian telescope which has been described in detail in SP89b. During the observations, the ellipsoidal secondary oscillated sinusoidally at 8 Hz with a peak-to-peak throw of 3° on the sky. The receiver signals were phase synchronously demodulated using a "square-wave" lock-in amplifier and sampled every 0.5 s. The beam profile of the telescope can be approximated as a Gaussian beam with a 1 σ_b dispersion which varies in frequency as given below. Two different total power radiometers were used in these observations. The lower frequency (Ka-band) receiver is similar to that described in SP91a and incorporates a very low noise, high electron mobility transistor (HEMT) amplifier (Pospieszalski, Gallego, & Lakatosh 1990) cooled to 4 K in a ^{4}He Dewar. This receiver operated at four center frequencies (27.25, 29.75, 32.25, and 34.75 GHz) with 2.5 GHz 3 dB bandwidths. The frequency subdivision is used to compensate for gain variations across the full band and to obtain spectral information which can be used to discriminate between the various astrophysical foregrounds. For the Ka-band system, the beam dispersion is given by $\sigma_b = 0°.70 \pm 0°.04 \times (27.7/\nu_{\rm GHz})$. The higher frequency receiver (Q-band) is described in Gundersen et al. (1994) and also uses a cryogenic HEMT amplifier based on a design developed at the National Radio Astronomy Observatory (NRAO). This amplifier was built at the University of California, Santa Barbara with assistance from NRAO and uses an AlInAs/GaInAs/InP HEMT (Pospieszalski et al. 1994) in the first of five amplification stages. The Q-band system was multiplexed into three equal channels centered at 39.15, 41.45, and 43.75 GHz with nominal 3 dB bandwidths of 2.3 GHz, and the beam dispersion is given by $\sigma_b = 0°.47 \pm 0°.04 \times (41.5/\nu_{\rm GHz})$. The HEMT ampli-

fiers introduce intrinsic cross-correlations between the channels which can be characterized by the correlation coefficient between any two frequencies. The measured correlations were typically 0.25 and 0.50 for the Ka and Q-band systems, respectively, including atmospheric correlations. The radiometers are calibrated to 10% absolute accuracy and 3% relative accuracy using a combination of cryogenic cold loads, the sky, ambient Eccosorb, and the Moon. The long-term stability of the system was checked daily by inserting an ambient load "calibrator." These calibrations varied by less than 3% over the timescale of an observation and contribute a negligible amount to the final error estimate.

3. OBSERVATIONS

Two observations were performed between 1994 January 9 and 1994 January 22, and collected 261 hr of data. The first observation used the Q-band receiver, and the second observation used the Ka-band receiver. These observations consisted of smooth, constant declination, constant velocity scans of length 20° on the sky about a center $\alpha_{cen} = 45°$, $\delta_{cen} = -62°$. The closest approach to the Sun was 60° on the sky, and the closest approach to the plane of the galaxy corresponds to $b^{II} = -40°$, $l^{II} = 272°$. This is a low foreground emission region which is near the region observed in SP91. A measurement of the η Carina region showed that the absolute elevation was 1° lower than expected. The offset has been attributed to sag in the inner frame of the telescope mount and makes a direct comparison between these measurements and the SP91 measurements not possible. The right ascension is given by $\alpha(t) = \alpha_{cen} + [20|2 \text{ int } (v_{sc}\, t/2) + 1 - v_{sc}\, t| - 10 + \alpha_0 \sin (2\pi v_{ch}\, t)]/\cos \delta_{cen}$, where $\alpha_0 = 1.^\circ 5$ is the sinusoidal chop amplitude, $v_{ch} = 8$ Hz is the chop frequency, and $v_{sc} = 10$ mHz is the scan frequency. The position on the sky is then given by $\varphi(t) = \alpha(t) \cos \delta_{cen}$. Observations of the Moon established the absolute pointing at low elevations, and this was confirmed with observations of the η Carina region at high elevations. The error in absolute pointing is $\pm 0.^\circ 25$ in right ascension and $\pm 0.^\circ 12$ in declination, while the error in relative pointing is $\pm 0.^\circ 05$ in right ascension and $\pm 0.^\circ 05$ in declination. The peak-to-peak roll angle about the secondary's nutation axis was measured to be less than $0.^\circ 01$ as a function of aximuth angle. For a constant declination observation, the dimensionless window function for the product of a temperature at position $\hat{n}_i^k$ and a temperature at position $\hat{n}_j^l$ is given by

$$W_\ell(\Phi_{ij}^{kl}) = B_\ell(\sigma_b^k) B_\ell(\sigma_b^l) \sum_{r=0}^{\ell} \frac{(2\ell - 2r)!(2r)!}{[2^\ell r!(\ell - r)!]^2} \times 4H_0^2[(\ell - 2r)\alpha_0] j_0^2\left[\frac{(\ell - 2r)\Delta\varphi}{2}\right] \cos [(\ell - 2r)\Phi_{ij}^{kl}] , \quad (1)$$

where $\Phi_{ij}^{kl} = \cos^{-1} (\hat{n}_i^k \cdot \hat{n}_j^l)$ is the angular difference (or lag) between the temperature measured at bin i with channel k and the temperature measured at bin j with channel l. The beam profile function is given by $B_\ell(\sigma_b) = \exp [-\ell(\ell + 1)\sigma_b^2/2]$, H_0 is the Struve function of 0 index, j_0 is the zeroth-order spherical Bessel function, and $\Delta\varphi = (20/43)(\pi/180)$ is the bin size in radians on the sky. The indices are given by $i, j = 1$ to $N = 43$ bins and $k, l = 1$ to $F = 3$ for the Q-band data and $k, l = 1$ to $F = 4$ for the Ka-band data. This window function is a specific example taken from a more general expression in White & Srednicki (1994).

4. DATA REDUCTION AND ANALYSIS

Data were rejected for a number of reasons, including poor pointing/chopper performance (1.2%), performance of other observations (0.2%), calibration sequences (0.7%), telescope/receiver maintenance (9.1%), temperature variations of the cold plate and back-end electronics (0.9%), and bad weather (12.9%). From a total of 261 hr of data, 196 hr were used in this analysis. The poor weather data were determined in a way similar to SP91b in which the data from a single scan were combined into position bins from which an average and 1 σ error bar were calculated. The χ^2 of the individual scans was then calculated, and if the probability of exceeding χ^2 for 43 degrees of freedom was less than 0.01 for any channel, then the data from *all* channels for that scan were removed. As a cross check, other weather filters similar to SP91a were also implemented with no significant changes in the final data set. As with SP89 and SP91, an offset and gradient were removed in time over the timescale of a single scan (100 s) for each of the channels in an observation. The offsets were between 1 and 2 mK depending on the channel. The offset and gradient subtraction are taken into account in the analysis by creating a matrix R such that $\tilde{T}_a^k = R_{aj}^{kl} T_j^l$, where T_j^l are the $F \times N$ temperature means and $\tilde{T}_a^k$ are the $F \times (N - 2)$ projected temperatures with $a = 1, N - 2$. The formation of R is discussed in Bunn et al. (1994), and we have made R orthogonal such that $R^T R = I$. The co-added means and 1 σ error bars are shown in Figure 1 and show statistically significant, correlated signals for each observation. All quoted temperatures have been converted from antenna temperature to thermodynamic temperature and have been corrected for atmospheric absorption. In order to determine the origin of the observed structure, the data were binned in azimuthal and heliocentric coordinate systems. Various subset analyses were performed including dividing the data set into four roughly equal quarters in time and dividing the data into four roughly equal quarters depending on the azimuthal position of the telescope beam. None of

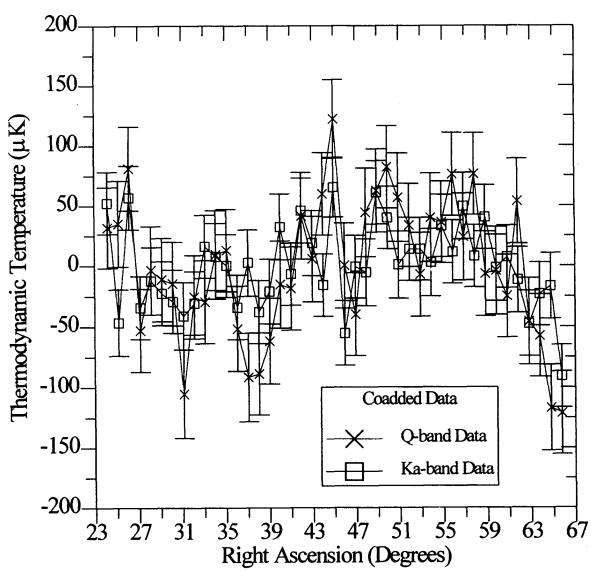

FIG. 1.—The individual channels from the independent Ka and Q-band observations have been co-added to produce the means and (± 1 σ) error bars shown here. The correlated structure in these two independent data sets from the same region of the sky ($\delta = -62°$) attests to the reproducibility of the observed signal. The error bars account for the channel-channel correlations.

these analyses suggest that the observed structure is anything but celestial in origin.

5. ASTROPHYSICAL FOREGROUNDS

There are several astrophysical foregrounds which could contaminate these observations. These include diffuse synchrotron and free-free emission from within our own Galaxy and extragalactic emission from discrete radio sources. Neither the Sunyaev-Zeldovich effect nor diffuse 20 K dust emission is expected to contribute more than a few μK signal. Using the 408 MHz map (Haslam et al. 1982) as a tracer of diffuse, high Galactic latitude synchrotron emission and a spectral index, $\beta = -2.8$ (such that the antenna temperature, $T_A \propto \nu^\beta$), we estimate that the diffuse synchrotron contribution to the observed rms is <7 μK in the lowest frequency channel and <3 μK in the highest frequency channel. The small amount of differential emission that exists in this region of the sky at 408 MHz can be correlated with discrete radio sources which have been observed in other source surveys at 408 MHz and are identified in the PKSCAT90 database (Wright & Otrupcek 1990). Unlike diffuse synchrotron emission, discrete radio sources and free-free emission cannot be dismissed on amplitude arguments alone. For diffuse free-free emission, there are no all-sky surveys which would allow a direct estimate of the free-free contribution to the observed structure. Instead, we have to rely on estimates based on a $10° \times 12°$ Hα map (Reynolds 1992) made at a similar angular scale to predict an average background free-free brightness temperature that can be expressed as $T_{\rm ff} = 1 \times 10^{-2} \nu_{\rm GHz}^{-2.1} \csc |b^{\rm II}|$. Reynolds's data suggests that the variations in the Hα intensity may be a factor of 2 above the average, such that $\Delta T_{\rm ff} = 2T_{\rm ff}$. From this we calculate the differential brightness temperature due to free-free emission (upon the closest approach to the Galactic plane) to range from $\Delta T_{\rm ff} = 30$ μK at the lowest frequency to $\Delta T_{\rm ff} = 12$ μK at the highest frequency. There have been many discrete source surveys at lower frequencies which are compiled in the PKSCAT90 database. The Parkes-MIT-NRAO (PMN) survey at 4.85 GHz (Wright et al. 1994) serves as the most sensitive survey with a flux limit of 30 mJy in our observation region and includes all the sources identified in PKSCAT90 for our region. The sensitivity of the telescope is 47 μK Jy^{-1} (assuming 100% aperture efficiency), so a 30 mJy flat spectrum source, with a flux density S(Jy) $\propto \nu^0$, would produce a 1.4 μK signal. This is well below the noise of the observations. If we make the worst-case assumption that all the point sources have flat spectra to 45 GHz, then we estimate that they would produce a $\Delta T_{\rm rms} = 15$–20 μK. Since the worst-case estimates of contamination from free-free emission and flat spectrum point sources are comparable to the rms level of the observed structure, we cannot dismiss or verify these types of foreground contamination without measuring β. This is addressed in the following likelihood analysis.

6. LIKELIHOOD ANALYSIS

We use the Bayesian method with a uniform prior (Bond et al. 1991) in the determination of the root mean square (rms) amplitude of the data and to make an estimate of the band power in the CMB power spectrum (Bond 1994). The experimental two-point correlation function is given by

$$C(\hat{n}_i^k \cdot \hat{n}_j^l) = \left\langle \frac{\Delta T(\hat{n}_i^k)\Delta T(\hat{n}_j^l)}{T_0^2} \right\rangle = \frac{1}{4\pi} \sum_{\ell=2}^{\infty} (2\ell + 1) C_\ell W_\ell(\Phi_{ij}^{kl}) , \quad (2)$$

where $\langle a_{\ell m} a_{\ell' m'} \rangle = \delta_{\ell\ell'} \delta_{mm'} C_\ell$ for a spherical harmonic expansion of the radiation temperature given by $\Delta T(\hat{n})/T_0 = \sum_{\ell m} a_{\ell m} Y_{\ell m}(\hat{n})$, W_ℓ is the window function (eq. [1]), and $T_0 = 2.726 \pm 0.01$ K (Mather et al. 1994). The rms amplitude is calculated from

$$\left(\frac{\Delta T}{T_0}\right)^2_{\rm rms} = \frac{1}{4\pi} \sum_{\ell=2}^{\infty} (2\ell + 1) C_\ell \overline{W}_\ell ,$$

$$\overline{W}_\ell = \frac{\sum_{i=j,kl} W_\ell(\Phi_{ij}^{kl})/(D_{ij}^{kl} \sigma_i^k \sigma_j^l)}{\sum_{i=j,kl} 1/(D_{ij}^{kl} \sigma_i^k \sigma_j^l)} , \quad (3)$$

where W_ℓ is the average window function at zero lag and $D_{ij}^{kl} \sigma_i^k \sigma_j^l$ is the data covariance matrix. The data covariance matrix is diagonal in each of the F^2 $N \times N$ submatrices and accounts for all spatial and channel-channel correlations as well as the error for each bin at each frequency. Following Bond (1994), the band power estimate is given by

$$\langle \mathscr{C}_\ell \rangle_B = \left\langle \frac{C_\ell \ell(\ell + 1)}{2\pi} \right\rangle_B = \frac{(\Delta T/T_0)^2_{\rm rms}}{\sum_{\ell=2}^{\infty} [\ell + (1/2)] \overline{W}_\ell / [\ell(\ell + 1)]} . \quad (4)$$

We consider a "flat" radiation power spectrum given by $C_\ell \propto (f^k f^l)^\beta / [\ell(\ell + 1)]$, where the constant of proportionality and β are determined in the likelihood analysis and f^k is the center frequency of channel k normalized to the lowest frequency of the observation(s). As given in Wollack et al. (1993) (SK93), the full covariance matrix is given by $M_{ij}^{kl} = C(\hat{n}_i^k \cdot \hat{n}_j^l) + D_{ij}^{kl} \sigma_i^k \sigma_j^l / T_0^2$. The offset and gradient subtraction are taken into account by creating a projected covariance matrix given by $\tilde{M} = RMR^T$, where R is defined in § 4. The likelihood of the data set is proportional to $|\tilde{M}|^{-1/2} \exp(-\chi^2/2)$, where $\chi^2 = \tilde{T}^T \tilde{M}^{-1} \tilde{T}$ for $F \times (N - 2)$ degrees of freedom. Table 1 lists the resulting rms and band power estimates for the individual observations as well as the combined observations. Figure 2 shows the band power estimates in relation to other recent measurements and a variety of theoretical power spectra.

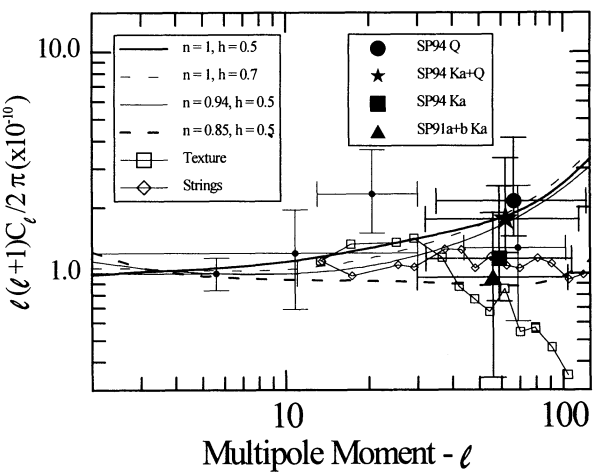

FIG. 2.—Band power estimates (± 1 σ) as given in Table 1 compared to a variety of theoretical power spectra and other recent low-ℓ measurements. Reading from low ℓ to high ℓ, the other measurements include *COBE*, the Far-Infrared Survey, Tenerife, and SK93. The higher ℓ measurements have not been included for clarity's sake but can be found in Bond (1994) along with complete citations. The horizontal error bars represent the FWHM of the given window function. The theoretical power spectra were provided by Steinhardt (1994).

TABLE 1

DERIVED PARAMETERS FROM LIKELIHOOD ANALYSIS ($\pm 1\ \sigma$)

Band (1)	ΔT_{rms} (μK) (2)	β (3)	ΔT_{rms} (μK) (4)	$\langle C_\ell \ell(\ell+1)/(2\pi)\rangle_B$ ($\times 10^{-10}$) (5)
Q-band	$43.1^{+16.9}_{-7.4}$	$1.7^{+1.5}_{-1.6}$	$49.6^{+19.4}_{-8.4}$	$2.14^{+2.00}_{-0.66}$
Ka-band.....	$30.5^{+14.7}_{-5.7}$	$0.2^{+0.9}_{-1.4}$	$31.9^{+14.7}_{-6.4}$	$1.17^{+1.33}_{-0.42}$
Ka + Q	$31.3^{+11.3}_{-6.0}$	$0.9^{+0.3}_{-0.6}$	$41.2^{+15.5}_{-6.7}$	$1.77^{+1.58}_{-0.53}$

NOTE.—Cols. (2)–(3): The rms amplitude and spectral index β determined from the likelihood analysis using a "flat" radiation power spectrum given by $C_\ell \propto (f^k f^l)^\beta/[\ell(\ell+1)]$, where f^k is the center frequency of channel k normalized to the lowest frequency of the observation. Col. (4): The rms amplitude for $\beta = 0$. Col. (5): CMB band power estimates for $\beta = 0$.

7. DISCUSSION

The band power estimates of the Ka and Q-band data are consistent with a range of theoretical power spectra (some of which are shown in Fig. 2) and do not independently reject any of the models. Due to the frequency-dependent beam size, a thermal point source would have a measured spectral index of $\beta = 2$ while a diffuse thermal source would have a measured spectral index of $\beta = 0$. Thus, the range of measured spectral indices given in Table 1 are all consistent with a CMB spectrum. Likewise, a flat spectrum point source would have a measured spectral index of $\beta = 0$, so the Ka and Q-band measurements do not strongly reject flat or inverted spectrum point sources. The combined Ka + Q data show a marked improvement on the 1 σ confidence interval for β and formally reject spectra with $\beta < -2$ (such a diffuse synchrotron and free-free emission) at the 5 σ level. The SP94 results are most easily compared to the SP91 results and the SK93 results. To date, no analysis of the SP91 results has included the channel-channel correlations. We have performed a reanalysis of the combined SP91a + b data using the method outlined in § 6, and it gives $\langle \mathscr{C}_\ell \rangle_B = 1.23^{+0.83}_{-0.41} \times 10^{-10}$ for $\beta = -5.2^{+1.2}_{-5.1}$. Although there is no independent evidence of foreground contamination, the data can be marginalized (Dodelson & Stebbins 1994) with respect to a $\beta = -3.0$ foreground, and this produces a slightly lower band power of $\langle \mathscr{C}_\ell \rangle_B = 0.96^{+0.93}_{-0.62} \times 10^{-10}$. A reanalysis of SP91b alone gives $\langle \mathscr{C}_\ell \rangle_B = 1.30^{+1.48}_{-0.53} \times 10^{-10}$ for $\beta = -3.6^{+1.2}_{-3.9}$. If the SP91b data is also marginalized with respect to a $\beta = -3.0$ foreground, a band power of $\langle \mathscr{C}_\ell \rangle_B = 0.88^{+1.53}_{-0.66} \times 10^{-10}$ is obtained. These band power estimates are smaller than, but consistent with, the SP94 results. The SK93 result gives $\langle \mathscr{C}_\ell \rangle_B = 1.31^{+1.2}_{-0.7} \times 10^{-10}$, for $\beta = -0.3^{+0.7}_{-1.2}$ which is also consistent with the SP94 results, although one should note the differences between the experiments which are addressed in SK93.

We would like to thank M. Pospieszalski, M. Balister, and W. Lakatosh of NRAO-CDL for useful information regarding amplifiers and for supplying the 26–36 GHz HEMT amplifier. In addition, we would like to thank L. Nguyen of Hughes Research Labs for providing the InP HEMTs which we have incorporated into our 38–45 GHz amplifiers. This project would have been impossible without the support of B. Sadoulet and the Center for Particle Astrophysics. D. Fischer and the whole Antarctic Support Associates staff provided the valuable support and expertise at the Amundsen-Scott South Pole station. We are grateful to R. Bond, M. Srednicki, P. Steinhardt, M. White, and L. Page and N. Sugiyama for useful discussions regarding data analysis and window functions. We would like to acknowledge the previous contributions of J. Schuster. N. F. is partially supported by Conselho Nacional de Desonvolvimento Cientifico e Tecnologico, Brazil. This work was supported by NSF grant OPP 92-21468 and AST 91-20005.

The means, covariances, and window functions will be made available from rot.ucsb.edu using anonymous FTP in the directory [sp94dat] and from the Web site http://www.deepspace.ucsb.edu.

REFERENCES

Bond, J. R. 1994, Ap. Lett. Comm.
Bond, J. R., et al. 1991, Phys. Rev. Lett., 66, 2179
Bunn, E., et al. 1994, ApJ, 429, L1
Dodelson, S., & Stebbins, A. 1994, ApJ, 433, 440
Gaier, T., et al. 1992, ApJ, 398, L1
Gundersen, J. O., et al. 1994, Proc. Case Western CMB Workshop, CMB Anisotropies: Two Years After *COBE*, ed. L. Krauss (Singapore: World Scientific), in press
Haslam, C. G. T., et al. 1982, A&AS, 47, 1
Lubin, P. M. 1994, Proc. IAU Symp. 168, ed. M. Kafatos & Y. Kondo (Dordrecht: Kluwer), in press
Mather, J., et al. 1994, ApJ, 420, 439
Meinhold, P., & Lubin, P. 1991, ApJ, 370, L11
Meinhold, P., et al. 1993, ApJ, 406, 12
Pospieszalski, M. W., Gallego, J. D., & Lakatosh, W. J. 1990, IEEE MTT-S Digest 1253
Pospieszalski, M. W., et al. 1994, Proc. International Microwave Symp., ed. H. J. Kuno (New York: IEEE), 1345
Reynolds, R. J. 1992, ApJ, 392, L35
Schuster, J., et al. 1993, ApJ, 412, L47
Smoot, G. F., et al. 1992, ApJ, 396, L1
Steinhardt, P. J. 1994, private communication
White, M., & Srednicki, M. 1994, ApJ, 443, 6
Wilkinson, D. 1994, Proc. 9th Lake Louise Winter Institute, Particle Physics and Cosmology, ed. A. Astbury et al. (Singapore: World Scientific), in press
Wollack, E. J., et al. 1993, ApJ, 419, L49
Wright, A. E., & Otrupcek, R. E., ed. 1990, ATNF, PKSCAT90: The Southern Radio Database (Sydney: ATNF)
Wright, A. E., et al. 1994, ApJS, 91, 111